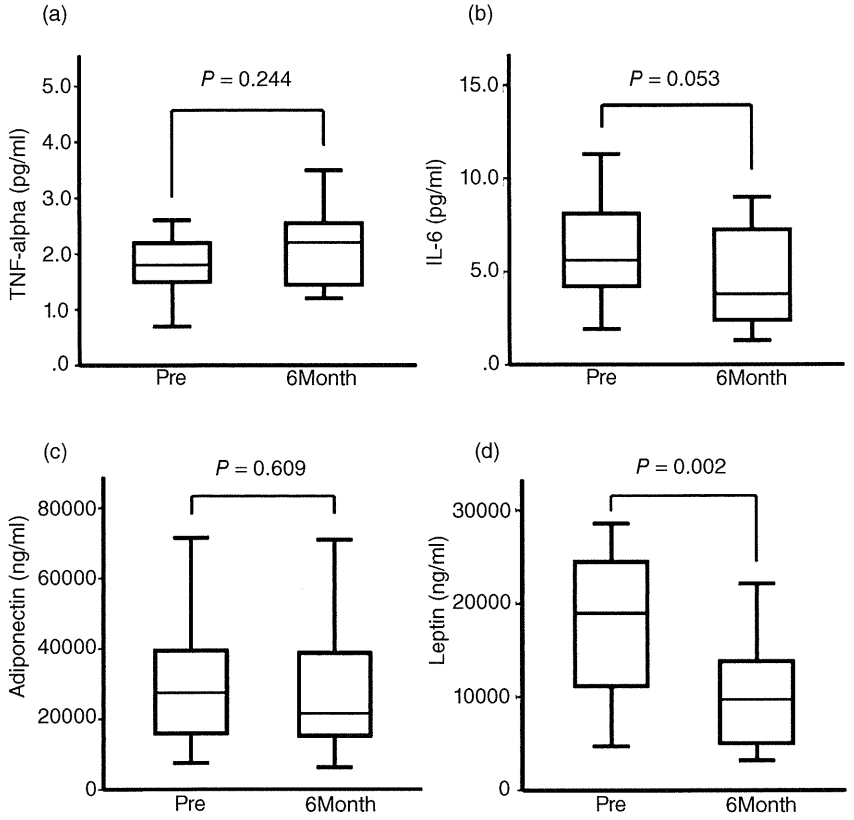

Figure 2 Changes in cytokines and adipokines after 6 months of exercise. (a) Tumor necrosis factor (TNF)-α, (b) interleukin (IL)-6 and (c) adiponectin did not significantly change, whereas levels of (d) leptin significantly decreased after 6 months of exercise ($P = 0.002$). "Pre", before the exercise period; "6Month", 6 months after starting exercise.

The exercise did not significantly improve the HRQOL. However, vitality tended to be improved. Because the number of patient was limited, we could not exclude the notion that exercise improved the HRQOL. However, we considered that the exercise would potentially improve vitality, which would relate to an improved HRQOL.

We recently reported that a diabetic profile in the 75-g oral glucose tolerance test[37] is a risk factor for HCC and the findings of another group[38] support this notion. The mechanism of hepatocarcinogenesis induced by diabetes mellitus in patients infected with HCV has not yet been determined. However, obesity, especially the accumulation of visceral fat, causes insulin resistance and leads to diabetes mellitus. Our data indicate that aerobic exercise such as walking can decrease the occurrence of HCC by decreasing body fat and improving insulin resistance. Exercise can have an important impact upon the prevention of HCC in patients infected with HCV because it is an inexpensive and practical measure compared with other alternatives, such as antiviral therapy. Moreover, obesity and insulin resistance are host factors that reduce the effectiveness of IFN.[9,39] Our data support the notion that aerobic exercise is a significant measure for increasing the effectiveness of IFN through improving obesity and insulin resistance.

We could not completely negate the influence of diet in the absence of comparison with a group treated only with dietary modification. However, our patients received only dietary instruction for 2 months and then they started the exercise to minimize the influence of diet. Furthermore, oral intake did not change during the study period. Those data would indicate that the improvements in insulin resistance and other metabolic factors were mainly affected by the exercise intervention. The exercise exerted an effect mostly in patients who achieved the target number of steps. Insulin resistance significantly improved among patients who achieved an average of 8000 steps/day. This finding indicated that this level of daily exercise is ideal for improving insulin

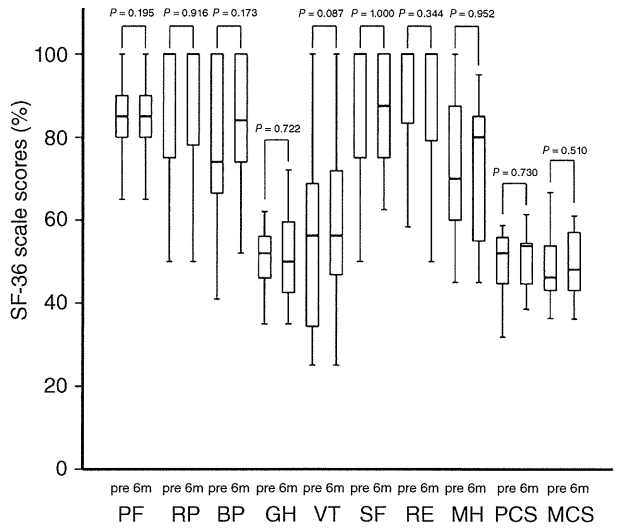

Figure 3 Short Form-36 (SF-36) scale scores. Vitality score tended to improve after exercise ($P = 0.087$). Other parameters did not significantly differ between before and after 6 months of exercise. PF, physical functioning; RP, role – physical; BP, bodily pain; GH, general health; VT, vitality; SF, social functioning; RE, role – emotional; MH, mental health; PCS, physical component summary; MCS, mental component summary. Values of pre (before exercise period) and of 6m (6 months after starting exercise) were compared in each group.

resistance, and that our protocol could evaluate the effectiveness of aerobic exercise.

In conclusion, walking as aerobic exercise improved insulin resistance and decreased body fat as well as serum levels of leptin in patients with HCV without worsening liver function. Exercise has the potential to increase the effect of IFN therapy and to decrease serum levels of leptin, which could be associated with HCC.

ACKNOWLEDGMENTS

THIS STUDY WAS supported in part by a Grant-in-Aid for Young Scientists (B) (JSPS KAKENHI 20700552), Ehime University Graduate School of Medicine Young Investigator Award (to I. K.), and by a Grant-in-Aid for Scientific Research (JSPS KAKENHI 21590848) (to Y. H.) from the Ministry of Education, Culture, Sports, Science and Technology, Japan.

REFERENCES

1 Ikeda K, Saitoh S, Suzuki Y *et al.* Disease progression and hepatocellular carcinogenesis in patients with chronic viral hepatitis: a prospective observation of 2215 patients. *J Hepatol* 1998; **28**: 930–8.
2 Niederau C, Lange S, Heintges T *et al.* Prognosis of chronic hepatitis C: results of a large, prospective cohort study. *Hepatology* 1998; **28**: 1687–95.
3 Kenny-Walsh E. Clinical outcomes after hepatitis C infection from contaminated anti-D immune globulin. Irish Hepatology Research Group. *N Engl J Med* 1999; **340**: 1228–33.
4 Caronia S, Taylor K, Pagliaro L *et al.* Further evidence for an association between non-insulin-dependent diabetes mellitus and chronic hepatitis C virus infection. *Hepatology* 1999; **30**: 1059–63.
5 Mason AL, Lau JY, Hoang N *et al.* Association of diabetes mellitus and chronic hepatitis C virus infection. *Hepatology* 1999; **29**: 328–33.
6 Shintani Y, Fujie H, Miyoshi H *et al.* Hepatitis C virus infection and diabetes: direct involvement of the virus in the development of insulin resistance. *Gastroenterology* 2004; **126**: 840–8.
7 Delgado-Borrego A, Jordan SH, Negre B *et al.* Reduction of insulin resistance with effective clearance of hepatitis C infection: results from the HALT-C trial. *Clin Gastroenterol Hepatol* 2010; **8**: 458–62.
8 Muzzi A, Leandro G, Rubbia-Brandt L *et al.* Insulin resistance is associated with liver fibrosis in non-diabetic chronic hepatitis C patients. *J Hepatol* 2005; **42**: 41–6.
9 Romero-Gomez M, Del Mar Viloria M, Andrade RJ *et al.* Insulin resistance impairs sustained response rate to peginterferon plus ribavirin in chronic hepatitis C patients. *Gastroenterology* 2005; **128**: 636–41.
10 Lo Iacono O, Venezia G, Petta S *et al.* The impact of insulin resistance, serum adipocytokines and visceral obesity on steatosis and fibrosis in patients with chronic hepatitis C. *Aliment Pharmacol Ther* 2007; **25**: 1181–91.
11 Gastaldelli A, Miyazaki Y, Mahankali A *et al.* The effect of pioglitazone on the liver: role of adiponectin. *Diabetes Care* 2006; **29**: 2275–81.
12 Nishitani S, Matsumura T, Fujitani S, Sonaka I, Miura Y, Yagasaki K. Leucine promotes glucose uptake in skeletal muscles of rats. *Biochem Biophys Res Commun* 2002; **299**: 693–6.
13 Nishitani S, Takehana K, Fujitani S, Sonaka I. Branched-chain amino acids improve glucose metabolism in rats with liver cirrhosis. *Am J Physiol Gastrointest Liver Physiol* 2005; **288**: 1292–300.
14 Friedman JM, Halaas JL. Leptin and the regulation of body weight in mammals. *Nature* 1998; **395**: 763–70.
15 Berg AH, Combs TP, Du X, Brownlee M, Scherer PE. The adipocyte-secreted protein Acrp30 enhances hepatic insulin action. *Nat Med* 2001; **7**: 947–53.
16 Arita Y, Kihara S, Ouchi N *et al.* Paradoxical decrease of an adipose-specific protein, adiponectin, in obesity. *Biochem Biophys Res Commun* 1999; **257**: 79–83.

17 Cua IH, Hui JM, Bandara P *et al.* Insulin resistance and liver injury in hepatitis C is not associated with virus-specific changes in adipocytokines. *Hepatology* 2007; **46**: 66–73.
18 Havel PJ, Kasim-Karakas S, Mueller W, Johnson PR, Gingerich RL, Stern JS. Relationship of plasma leptin to plasma insulin and adiposity in normal weight and overweight women: effects of dietary fat content and sustained weight loss. *J Clin Endocrinol Metab* 1996; **81**: 4406–13.
19 Solomon TP, Sistrun SN, Krishnan RK *et al.* Exercise and diet enhance fat oxidation and reduce insulin resistance in older obese adults. *J Appl Physiol* 2008; **104**: 1313–19.
20 Snowling NJ, Hopkins WG. Effects of different modes of exercise training on glucose control and risk factors for complications in type 2 diabetic patients: a meta-analysis. *Diabetes Care* 2006; **29**: 2518–27.
21 Courneya KS, Sellar CM, Stevinson C *et al.* Randomized controlled trial of the effects of aerobic exercise on physical functioning and quality of life in lymphoma patients. *J Clin Oncol* 2009; **27**: 4605–12.
22 Courneya KS, Mackey JR, Bell GJ, Jones LW, Field CJ, Fairey AS. Randomized controlled trial of exercise training in postmenopausal breast cancer survivors: cardiopulmonary and quality of life outcomes. *J Clin Oncol* 2003; **21**: 1660–8.
23 Ritland S, Foss NE, Gjone E. Physical activity in liver disease and liver function in sportsmen. *Scand J Soc Med Suppl* 1982; **29**: 221–6.
24 Bonora E, Formentini G, Calcaterra F *et al.* HOMA-estimated insulin resistance is an independent predictor of cardiovascular disease in type 2 diabetic subjects: prospective data from the Verona Diabetes Complications Study. *Diabetes Care* 2002; **25**: 1135–41.
25 Fukuhara SSY, Bito S, Kurokawa K. *Manual of SF-36, Japanese Version 1.2*. Tokyo: Public Health Research Foundation, 2001.
26 Senn JJ, Klover PJ, Nowak IA, Mooney RA. Interleukin-6 induces cellular insulin resistance in hepatocytes. *Diabetes* 2002; **51**: 3391–9.
27 Senn JJ, Klover PJ, Nowak IA *et al.* Suppressor of cytokine signaling-3 (SOCS-3), a potential mediator of interleukin-6-dependent insulin resistance in hepatocytes. *J Biol Chem* 2003; **278**: 13740–6.
28 Gielen S, Adams V, Mobius-Winkler S *et al.* Anti-inflammatory effects of exercise training in the skeletal muscle of patients with chronic heart failure. *J Am Coll Cardiol* 2003; **42**: 861–8.
29 Romero-Gomez M, Castellano-Megias VM, Grande L *et al.* Serum leptin levels correlate with hepatic steatosis in chronic hepatitis C. *Am J Gastroenterol* 2003; **98**: 1135–41.
30 Brabant G, Muller G, Horn R, Anderwald C, Roden M, Nave H. Hepatic leptin signaling in obesity. *FASEB J* 2005; **19**: 1048–50.
31 Ribatti D, Belloni AS, Nico B, Di Comite M, Crivellato E, Vacca A. Leptin-leptin receptor are involved in angiogenesis in human hepatocellular carcinoma. *Peptides* 2008; **29**: 1596–602.
32 Saxena NK, Sharma D, Ding X *et al.* Concomitant activation of the JAK/STAT, PI3K/AKT, and ERK signaling is involved in leptin-mediated promotion of invasion and migration of hepatocellular carcinoma cells. *Cancer Res* 2007; **67**: 2497–507.
33 Ikejima K, Takei Y, Honda H *et al.* Leptin receptor-mediated signaling regulates hepatic fibrogenesis and remodeling of extracellular matrix in the rat. *Gastroenterology* 2002; **122**: 1399–410.
34 Yang WS, Lee WJ, Funahashi T *et al.* Weight reduction increases plasma levels of an adipose-derived anti-inflammatory protein, adiponectin. *J Clin Endocrinol Metab* 2001; **86**: 3815–19.
35 Hulver MW, Zheng D, Tanner CJ *et al.* Adiponectin is not altered with exercise training despite enhanced insulin action. *Am J Physiol Endocrinol Metab* 2002; **283**: 861–5.
36 Garcia-Pagan JC, Santos C, Barbera JA *et al.* Physical exercise increases portal pressure in patients with cirrhosis and portal hypertension. *Gastroenterology* 1996; **111**: 1300–6.
37 Konishi I, Hiasa Y, Shigematsu S *et al.* Diabetes pattern on the 75 g oral glucose tolerance test is a risk factor for hepatocellular carcinoma in patients with hepatitis C virus. *Liver Int* 2009; **29**: 1194–201.
38 Veldt BJ, Chen W, Heathcote EJ *et al.* Increased risk of hepatocellular carcinoma among patients with hepatitis C cirrhosis and diabetes mellitus. *Hepatology* 2008; **47**: 1856–62.
39 Bressler BL, Guindi M, Tomlinson G, Heathcote J. High body mass index is an independent risk factor for nonresponse to antiviral treatment in chronic hepatitis C. *Hepatology* 2003; **38**: 639–44.

Original Paper

Transcatheter Arterial Chemoembolization with Fine-Powder Cisplatin-Lipiodol for HCC

Yohei Koizumi, Masashi Hirooka, Takahide Uehara, Yoshiyasu Kisaka, Kazuhiro Uesugi, Teru Kumagi, Masanori Abe, Bunzo Matsuura, Yoichi Hiasa and Morikazu Onji
Department of Gastroenterology and Metabology, Ehime University Graduate School of Medicine, Ehime, Japan
Corresponding Author: Yoichi Hiasa, MD, PhD; Department of Gastroenterology and Metabology, Ehime University Graduate School of Medicine, Shitsukawa, Toon, Ehime 791-0295, Japan
Tel: +81899605308, Fax: +81899605310, E-mail: hiasa@m.ehime-u.ac.jp

ABSTRACT

Background/Aims: Fine-powder cisplatin has recently been developed, allowing the easy manufacture of high-density cisplatin-lipiodol suspensions. The aim of this study is to evaluate the efficacy and toxicity of transcatheter arterial chemoembolization (TACE) with fine-powder cisplatin and lipiodol suspension against advanced hepatocellular carcinoma (HCC).
Methodology: We prospectively analyzed 20 patients (16 men, 4 women) with inoperative advanced HCC without extrahepatic metastases who underwent TACE with fine-powder cisplatin and lipiodol suspension in our hospital between August 2006 and December 2008. All patients were administered a suspension of fine-powder cisplatin at 10mg/1cm of tumor diameter.
Results: Partial response was seen in 10 cases, with stable disease in 7 cases and progressive disease in 3 cases. Overall response rate was 50%. The 1-year survival rate was 90%. Adverse effects (≥grade 3) occurred in 40%, with vomiting in 5%, thrombocytopenia in 15%, elevated serum bilirubin in 20%, decreased serum albumin in 5%, fever in 65%, general fatigue in 15% and anorexia in 30%. However, no other life-threatening, adverse events were observed.
Conclusion: TACE with fine-powder cisplatin suspended in lipiodol provides better therapeutic efficacy, suggesting the potential usefulness of this agent in the treatment of advanced HCC.

KEY WORDS: Cisplatin; Transcatheter arterial chemoembolization; Hepatocellular carcinoma

ABBREVIATIONS: Hepatocellular Carcinoma (HCC); Transcatheter Arterial Chemoembolization (TACE); Computed Tomography (CT); Response Evaluation Criteria in Solid Tumors (RECIST); Complete Response (CR); Partial Response (PR); Stable Disease (SD); Progressive Disease (PD); Response Rate (RR)

INTRODUCTION

After the diagnosis of hepatocellular carcinoma (HCC), patients can be treated with various procedures for HCC. Among these, transcatheter arterial chemoembolization (TACE) is performed for cases in which a radical cure seems likely to prove difficult. However, for TACE treatment, no clear evidence is available as to what kinds of anticancer agent should be used. In previous reports of TACE with anticancer agents to treat HCC, the response rate for doxorubicin was 35%. The 1-year survival rate was 82%, and the 2-year survival rate was 63% (1). These results are not satisfactory.

Conversely, with intra-arterial infusion therapy, response rates were 16.8% to doxorubicin (2), 15.1% to epirubicin (3) and 25% to mitomycin C (4). In recent years, cisplatin has been identified as an effective agent, and has been used for the treatment of HCC (5). The response rate to intra-arterial infusion therapy with cisplatin was 32.6% (6), representing a significant increase compared to other agents. More curative effects might thus be expected using cisplatin for TACE.

Few previous studies have examined TACE using a cisplatin-lipiodol suspension. One reason is that manufacturing a high-density cisplatin-lipiodol suspension is difficult. Fine-powder cisplatin has recently been developed, allowing the easy manufacture of high-density suspensions. We performed a prospective clinical phase II study to perform TACE using fine-powder cisplatin suspended in lipiodol, and then evaluated the therapeutic efficacy and safety of this treatment in patients with HCC.

METHODOLOGY

Patients

We prospectively analyzed 20 patients (16 men, 4 women) with HCC who underwent TACE with fine-powder cisplatin and lipiodol suspension in our hospital between August 2006 and December 2008. HCC patients who were diagnosed clinically as unresectable HCC by histology or by imaging such as computed tomography, and who provided written informed consent to participate in the study after being given a thorough explanation about the purposes and protocols of the study were enrolled. These patients were offered alternative treatment if they chose not to participate in the study. The study protocol conformed to the ethical guidelines of the 1975 Declaration of Helsinki. All study protocols were approved by the Institutional Review Board at Ehime University Hospital.

Hepato-Gastroenterology 2011; 58:1-6

Treatment schedule

We used the fine-powder formation of cisplatin (IA-call®; Nipponkayaku, Tokyo, Japan). Cisplatin was completely dissolved in 5mL of lipiodol and heated to 50°C, then a cisplatin-lipiodol suspension was obtained with a final cisplatin concentration of 10mg/mL. A catheter was introduced into the hepatic artery under angiographic guidance using the Seldinger technique. The drug was administered at a dose of 10mg/cm of tumor diameter. A substance with thrombotic effects, such as gelatin sponge, was concomitantly used for the treatment of HCC. Before and after drug administration, adequate hydration by intravenous drip infusion of 1000-2000mL of physiological saline was performed to prevent kidney damage. If necessary, we administered a diuretic and tried to secure the volume of urine. Hydration continued in principle for 3 days. Due to the potentially high incidence of nausea and vomiting, a 5-hydroxytriptamine (5-HT3) receptor antagonist was administered prophylactically.

Response and toxicity evaluation

Response rate was evaluated by comparison with findings on contrast-enhanced computed tomography (CT) obtained immediately before treatment. The CT findings were evaluated by two hepatologists. Direct and total effects on tumors were evaluated 3 and 6 months after TACE, respectively. We classified patients to the Response Evaluation Criteria in Solid Tumors (RECIST ver.1.1) guidelines (7) at 3 months after TACE, and defined complete response (CR), partial response (PR), stable disease (SD) and progressive disease (PD) at 6 months after TACE according to the parameters. Response rate (RR) was identified as the number of cases with CR or PR divided by the total number of patients in a group. We evaluated the response to treatment for the total group, as well for patients divided into those receiving initial treatment (initial treatment group, n=5) and those receiving treatment for recurrence (recurrence group, n=15). We also evaluated antitumor effects based on RECIST guidelines. Treatment safety was evaluated on the basis of the National Cancer Institute Common Toxicity Criteria version 3.

Statistical design

This study was performed prospectively, and statistical analysis for the comparison of backgrounds between the initial treatment and recurrence groups was performed using the Wilcoxon test. Moreover, comparisons of treatment efficacy and toxicity in each patient group were performed using the χ^2 test. JMP version 7 statistical software (SAS Institute Japan, Tokyo, Japan) was used for these analyses.

RESULTS

Patient characteristics

Patient background factors are shown in **Table 1**. Median patient age was 64.8 years (range, 54-82 years). All patients showed underlying liver cirrhosis. No significant differences in background factors were seen between groups by Wilcoxon test.

Therapeutic efficacy

Results of therapeutic efficacy are shown in **Table 2**, with CR in 0 cases (0%), PR in 10 cases (50%), SD in 7 cases (35%) and PD in 3 cases (15%). Overall response rate was 50%, and 1- and 2-year

TABLE 1 Patient Characteristics

Characteristics	n (%)	
No. patients	20	
Gender		
Male	16	(80.0)
Female	4	(20.0)
Age (mean ± SD)	64.8 ± 7.2 years	
Virus marker		
HBV+	3	(15.0)
HCV+	15	(75.0)
HBV+/HCV+		
HBV-/HCV-	3	(15.0)
Stage (1)		
II	17	(85.0)
III	3	(15.0)
ECOG performance status		
0	17	(85.0)
1	3	(15.0)
Child classification		
A	15	(75.0)
B	5	(25.0)

(1) UICC 1987 TNM Classification of Malignant Tumors, 4th edition. ECOG, Eastern Cooperative Oncology Group; HBV, hepatitis B virus; HCV, hepatitis C virus.

TABLE 2 Therapeutic Efficacy in the Present Study

	Initial treatment group (n=5)	Recurrence group (n=15)	Total (n=20)
CR	0	0	0
PR	2	8	10
SD	3	4	7
PD	0	3	3
RR	40%	53.3%	50%
1-year survival rate	80%	93.3%	90%
2-years survival rate	80%	85.6%	83.6%

RR, response rate; CR, complete response; PR, partial response; SD, stable disease; PD, progressive disease

survival rates were 90% and 83.6% (**Table 3**). The initial treatment group showed CR in 0 cases, PR in 2 cases, SD in 3 cases and PD in 0 cases (overall response rate, 40%). The recurrence group showed CR in 0 cases, PR in 8 cases, SD in 4 cases and PD in 3 cases (overall response rate, 53.3%). In terms of therapeutic efficacy, no significant difference was seen between groups (χ^2 test, p=0.76).

Adverse events

Side effects encountered in this study are shown in **Table 4**. Fever was seen in 13 cases (65%), vomiting in 1 case (5%), thrombocytopenia in 3 cases (15%), elevated serum bilirubin in 4 cases (20%), decreased serum albumin in 1 case (5%), general fatigue in 3 cases (15%) and anorexia in 6 cases (30%). The initial treatment group showed fever in 2 cases, general fatigue in 1 case, anorexia in 1 case, thrombocytopenia in 3 cases, elevated serum bilirubin in 3 cases and decreased serum albumin in 1 case.

The recurrence group showed fever in 11 cases, general fatigue in 2 cases, anorexia in 5 cases, vomiting in 1 case, thrombocytopenia in 2 cases and elevated serum bilirubin in 1 case. No significant differences in frequencies of adverse events were seen between groups according to the χ^2 test.

DISCUSSION

This study evaluated the efficacy and toxicity of TACE with fine-powder cisplatin and lipiodol suspension in 20 patients with advanced HCC. The overall response rate was 50%, with 1- and 2-year survival rates of 90% and 83.6%, respectively. In previous reports of TACE with anticancer agents to treat HCC, response rates to doxorubicin were 33-38% (**Table 3**). The 1-year survival rates were 24-82%, and 2-year survival rates were 31-63%. TACE with fine-powder cisplatin and lipiodol thus appears to offer better therapeutic value than TACE with epirubicin-lipiodol or doxorubicin-lipiodol performed generally.

TABLE 3 Comparison of Reported Chemotherapies for Hepatocellular Carcinoma

	Therapy	RR	1-year survival rate	2-year survival rate
Epirubicin Study Group (3) (1987)	Hepatic arterial infusion (Epirubicin)	15.1%	24%	-
Mäkelä *et al.* (4) (1993)	Hepatic arterial infusion (Mitomycin C)	25%	40%	-
Yoshikawa *et al.* (6) (2008)	Hepatic arterial infusion (Cisplatin with lipiodol)	33.8%	67.5%	50.8%
Pelletier *et al.* (13) (1990)	Chemoembolization (gelatin sponge plus doxorubicin)	33%	24%	-
Ono et al. (9) (2000)	Chemoembolization (gelatin sponge plus doxorubicin with lipiodol)	38%	50%	31%
Llovet *et al.* (1) (2002)	Chemoembolization (gelatin sponge plus doxorubicin)	35%	82%	63%
Present study	Chemoembolization (gelatin sponge plus cisplatin with lipiodol)	50%	90%	83.6%

RR, response rate

TABLE 4 Adverse Events

	Initial treatment group			Recurrence group			Total		
	All grades	Grade[1)] 2	3	All grades	Grade[1)] 2	3	All grades	Grade[1)] 2	3
Fever	2	1	0	11	0	0	13	1	0
Anorexia	1	0	0	5	0	0	6	0	0
Fatigue	1	0	0	2	0	0	3	0	0
Vomiting	0	0	0	1	0	0	1	0	0
Thrombocytopenia	1	0	1	2	0	2	3	0	3
Elevated total bilirubin	3	0	3	1	0	1	4	0	4
Decreased albumin	1	0	1	0	0	0	1	0	1

1) National Cancer Institute-Common Toxicity Criteria version 3.

Adverse events of TACE with cisplatin in past reports have included vomiting in 35-62%, anorexia in 93% and general fatigue in 28-84% using the cisplatin-lipiodol suspension (8-12). In our cases, vomiting was seen in 5%, anorexia in 30%, and general fatigue in 15%. The ratios of vomiting and anorexia were clearly lower in comparison with past reports. Among the side effects of TACE with cisplatin-lipiodol suspension, thrombocytopenia is characteristic. Thrombocytopenia has been reported in 33-35% of treated patients in past reports (10, 12), compared to 15% in our study. No reductions in renal function or harmful phenomena such as liver failure were observed in the present investigation. In all cases, no aggravation of solidification ability such as extension of prothrombin time was seen. On the basis of the above-mentioned results, we considered that the side effects resulting from TACE with cisplatin-lipiodol suspension were acceptable.

Fukushima *et al.* reported platinum concentrations in tissue after administering cisplatin-lipiodol suspension and aqueous cisplatin solution (12). When aqueous cisplatin was administered, concentrations of cisplatin between tumor and non-tumor did not differ significantly. However, when cisplatin-lipiodol suspension was administered, concentrations of cisplatin were 11.5-fold higher in tumor tissue than in non-tumor tissue. Lipiodol could thus offer a useful carrier for anti-cancer agents when delivered intra-arterially, due to selective accumulation in tumors. By blending cisplatin with lipiodol, we can decrease the outflow of cisplatin to the plasma compartment, with a resulting decrease in side effects. Moreover, in past studies, cisplatin powder was produced in the hospital by evaporating water and sodium chloride from the cisplatin solution. This may provide an inferior fine-powder form of cisplatin in terms of particle diameters, elution characteristics and stability. The commercial release of a fine-powder formulation of cisplatin appears to have resolved these problems, and has made uniform cisplatin-lipiodol suspensions easy to create. Such improvements will contribute to the efficacy of treatment, and eventually contribute to the prognosis of patients with HCC.

We studied the therapeutic efficacy of TACE with fine-powder cisplatin and lipiodol suspension and confirmed better curative effects. We will continue with this therapy for patients with HCC, and need to evaluate the prognosis in future analyses.

REFERENCES

1. **Llovet JM, Real MI, Montana X, et al:** Arterial embolisation or chemoembolisation versus symptomatic treatment in patients with unresectable hepatocellular carcinoma: a randomised controlled trial. Lancet 2002; 359:1734-1739.
2. **Ogawa M, Kurita S, Nishimura J, et al:** Clinical trials with adriamycin, a new antibiotic, in treatment of malignant neoplasms. Gan No Rinsho 1972; 18:806-813. (In Japanese).
3. **Epirubicin Study Group:** Intra-arterial administration of epirubicin in the treatment of nonresectable hepatocellular carcinoma. Epirubicin Study Group for Hepatocellular Carcinoma. Cancer Chemother Pharmacol 1987; 19:183-189.
4. **Mäkelä JT, Kantola R, Kairaluoma MI:** Superselective intra-arterial chemotherapy with mitomycin C for hepatocellular carcinoma. Surg Oncol 1993; 2:99-104.
5. **Uyama N, Hatano E, Maetani Y, et al:** Efficacy and toxicity of transcatheter arterial chemoembolization with cisplatin suspended in lipiodol for unresectable hepatocellular carcinoma. Jpn J Cancer Chemother 2008; 35:775-780. (In Japanese).
6. **Yoshikawa M, Ono N, Yodono H, et al:** Phase II study of hepatic arterial infusion of a fine-powder formulation of cisplatin for advanced hepatocellular carcinoma. Hepatol Res 2008; 38:474-483.
7. **Eisenhauer EA, Therasse P, Bogaerts J, et al:** New response evaluation criteria in solid tumours: revised RECIST guideline (version 1.1). Eur J Cancer 2009; 45:228-247.
8. **Shibata J, Fujiyama S, Sato T, et al:** Hepatic arterial injection chemotherapy with cisplatin suspended in an oily lymphographic agent for hepatocellular carcinoma. Cancer 1989; 64:1586-1594.
9. **Ono Y, Yoshimasu T, Ashikaga R, et al:** Long-term results of lipiodol-transcatheter arterial embolization with cisplatin or doxorubicin for unresectable hepatocellular carcinoma. Am J Clin Oncol 2000; 23:564-568.
10. **Kamada K, Nakanishi T, Kitamoto M, et al:** Long-term prognosis of patients undergoing transcatheter arterial chemoembolization for unresectable hepatocellular carcinoma: comparison of cisplatin lipiodol suspension and doxorubicin hydrochloride emulsion. J Vasc Interv Radiol 2001; 12:847-854.
11. **Maeda S, Shibata J, Fujiyama S, et al:** Long-term follow-up of hepatic arterial chemoembolization with cisplatin suspended in iodized oil for hepatocellular carcinoma. Hepatogastroenterology 2003; 50:809-813.
12. **Ikeda M, Maeda S, Shibata J, et al:** Transcatheter arterial chemotherapy with and without embolization in patients with hepatocellular carcinoma. Oncology 2004; 66:24-31.
13. **Pelletier G, Roche A, Ink O, et al:** A randomized trial of hepatic arterial chemoembolization in patients with unresectable hepatocellular carcinoma. J Hepatol 1990; 11:181-184.

EXPERIMENTAL CELL RESEARCH 317 (2011) 1851–1859

available at www.sciencedirect.com

ScienceDirect

www.elsevier.com/locate/yexcr

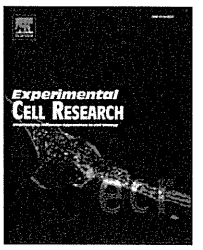

Research Article

ZNF689 suppresses apoptosis of hepatocellular carcinoma cells through the down-regulation of Bcl-2 family members

Shuichiro Shigematsu[a,b], *Shinji Fukuda*[b], *Hironao Nakayama*[b], *Hirofumi Inoue*[b,d], *Yoichi Hiasa*[a,c], *Morikazu Onji*[a], *Shigeki Higashiyama*[b,c,d,*]

[a] *Department of Gastroenterology and Metabology, Ehime University Graduate School of Medicine, Ehime, Japan*
[b] *Department of Biochemistry and Molecular Genetics, Ehime University Graduate School of Medicine, Ehime, Japan*
[c] *Department of Cell Growth and Tumor Regulation, Proteo-Medicine Research Center (ProMRES), Ehime, Japan*
[d] *Bioimaging Core Laboratory, Proteo-Medicine Research Center (ProMRES), Ehime, Japan*

ARTICLE INFORMATION

Article Chronology:
Received 18 January 2011
Revised version received 19 April 2011
Accepted 13 May 2011
Available online 20 May 2011

Keywords:
ZNF689
Hepatocellular carcinoma
Apoptosis
Zinc finger transcription factor

ABSTRACT

ZNF689, a C2H2-type of zinc finger transcription factor, was suggested to play a key role in hepatocarcinogenesis. However, none of the target genes or potential roles of ZNF689 in hepatocellular carcinoma (HCC) have been elucidated. Here, we investigated the role of ZNF689 in HCC cell lines focusing on cell viability and apoptosis. We found that the knockdown of ZNF689 by its specific siRNA decreased cell viability of Huh7. Cell cycle analysis revealed that the ZNF689 knockdown increased the proportion of the sub-G1 population, accompanied by an increase of annexin V- and TUNEL-positive cells. Western blot analysis revealed that ZNF689 knockdown induced the expression of pro-apoptotic factors of Bcl-2 family, Bax, Bak and jBid. There was a correlation between the expression of ZNF689 and an anticancer drug 5-fluorouracil (5-FU) resistance of HCC cells. *In vivo*, ZNF689 siRNA reduced tumor viability in HepG2-bearing mice with statistical significance. Furthermore, immunohistochemical analysis demonstrated that nuclei of a significant portion of human HCC surgical specimens were positive for ZNF689. Taken together, our results indicate that ZNF689 blocks pro-apoptotic signaling by suppressing the Bak/Bax/Bid pathway, resulting in the progression of liver cancer and resistance to 5-FU. ZNF689 may be a promising chemotherapeutic target against liver cancer.

Introduction

Hepatocellular carcinoma (HCC) is one of the most common cancers worldwide [1]. Surgical resection, liver transplantation, and percutaneous ablation offer the best prognosis for long-term survival [2]. Unfortunately, most HCC patients are diagnosed at advanced stages, when they are not suitable for curative operations due to extensive disease or severe liver dysfunction [3]. Although chemotherapy is an alternative choice as a multimodal treatment for advanced HCC, there is no generally accepted standard chemotherapy regimen, because of the low sensitivity and/or drug resistance to anticancer agents.

A crucial step to establish new strategies for cancer treatment is the identification of molecules that drive enhanced proliferation accompanied by a reduced rate of cell death. A common finding in chronic inflammatory liver disease and in HCC is the activation of growth factor expression and signaling. Among the relevant growth factors and their receptors to hepatocarcinogenesis are epidermal growth factor (EGF) family members such as heparin-binding EGF (HB-EGF), amphiregulin and transforming

* *Corresponding author at:* Department of Biochemistry and Molecular Genetics, Ehime University Graduate School of Medicine, Shitsukawa, Toon, Ehime 791-0295, Japan. Fax: +81 89 960 5256.
E-mail address: shigeki@m.ehime-u.ac.jp (S. Higashiyama).

0014-4827/$ – see front matter © 2011 Elsevier Inc. All rights reserved.
doi:10.1016/j.yexcr.2011.05.012

growth factor-α (TGF-α), and the EGF receptor (EGFR) [4]. We previously reported the enhanced expression of HB-EGF in HCC [5]. Recently, we identified promyelocytic leukemia zinc finger protein (PLZF) and its related factor B-cell leukemia 6 (Bcl6) as binding partners of C-terminal domain of membrane-anchored HB-EGF (proHB-EGF), which regulate multiple factors essential for cell cycle progression such as c-Myc, cyclin A, and cyclin D [6–8]. Both PLZF and Bcl6 contain tandem repeats of the Krüppel-like C2H2-type zinc finger domain at their carboxyl-terminal regions. A comprehensive oncogenomic database for HCC, OncoDB.HCC [9], indicates that more than 10 C2H2-type zinc finger proteins are expressed, some of which might play key roles in hepatocarcinogenesis.

In this study, we focused on one of these putative transcription factors, ZNF689, which is a recently identified C2H2-type of Krüppel-associated box (KRAB)-zinc finger protein specifically expressed in HCC but not in noncancerous liver tissues [10]. The previous study showed that over-expression of ZNF689 conferred anchorage-independent growth of NIH3T3 cells, and that knockdown of ZNF689 in HCC resulted in their growth inhibition [10], suggesting a key role in hepatocarcinogenesis. However, the molecular mechanism of ZNF689 function still remains unknown. Here we show that ZNF689 suppressed apoptotic signaling through down-regulation of apoptosis-promoting factors Bak/Bax/Bid, and suggest that molecular targeting of ZNF689-mediated anti-apoptotic effects may be an effective therapeutic strategy for HCC treatment.

Materials and methods

Cell culture

Huh7, HepG2, and Hep3B were obtained from the Health Science Research Resources Bank (HSRRB, Osaka, Japan) and cultured in Dulbecco's modified Eagle's medium supplemented with 10% fetal bovine serum, 100 units/ml penicillin and 10 μg/ml streptomycin in a humidified incubator with 5% CO_2 at 37 °C. 5-FU was purchased from Wako Pure Chemical Industries (Osaka, Japan). Nutlin-3 was purchased from Cayman Chemical (Ann Arbor, MI, USA).

Plasmid construction

Total RNA of Huh7 was extracted by TRIzol reagent (Invitrogen, Carlsbad, CA, USA), and used for the amplification of ZNF689 cDNA by the SuperScript RT III enzyme (Invitrogen). The entire coding region of ZNF689 was cloned into the expression vector pME18S-FLAG-NT. Lentiviruses used in this study were constructed by inserting cDNAs encoding ZNF689 or the stable luciferase green (SLG) from pSLG HSVTK control (TOYOBO, Osaka, Japan) into lentiviral expression vectors CSII-EF-MCS-IRES2-Venus and CSII-CMV-MCS-IRES2-Bsd (kindly provided by Dr. Miyoshi, RIKEN Bioresouce Center, Tsukuba, Japan).

qPCR analysis

For the expression profiling of apoptosis-related genes, RT2 Profiler PCR Array Human apoptosis (SABiosciences, Frederick, MD, USA) was used. qPCR was performed with the POWER SYBR Green PCR Master Mix and a 7300 Real-time PCR System (Applied Biosystems, Foster City, CA, USA) according to the manufacturer's protocol. Primer sequences used for qPCR were as follows:

GAPDH forward, 5′-TGCACCACCAACTGCTTAGC-3′;
GAPDH reverse, 5′-GGCATGGACTGTGGTCATGAG-3′;
ZNF689 forward, 5′-TGGAACGAAACACCGATGACT-3′;
ZNF689 reverse, 5′-CCATTCTTCTTTCTGGTTCTGCT-3′;
Bak forward, 5′-GAACAGGAGGCTGAAGGGGT-3′;
Bak reverse, 5′-TCAGGCCATGCTGGTAGACG-3′;
Bax forward, 5′-GCTGTTGGGCTGGATCCAAG-3′;
Bax reverse, 5′-TCAGCCCATCTTCTTCCAGA-3′.

Cell proliferation assay

Cell viability was quantified by a WST-1 colorimetric assay (Roche Applied Science, Basel, Switzerland). Briefly, 2×10^3 cells were seeded in 96-well plates. At each time point, cells were treated with WST-1 reagent and incubated for 120 min. The absorbance at 450 nm was recorded.

Gene silencing with small interfering RNA (siRNA)

siRNA cocktail against ZNF689 was purchased from B-Bridge International (Cupertino, CA, USA). HCC cells were transfected with the control or ZNF689 siRNA (5 nM for Huh7 and 20 nM for HepG2 and Hep3B) by Lipofectamine RNAiMax (Invitrogen) according to the instruction manual. The knockdown efficiency was validated by qPCR and Western blot analyses.

Detection of cell death

Early apoptosis was quantified using an Annexin V-FITC kit (Beckman Coulter, Brea, CA, USA) and 7-amino-actinomycin D (7-AAD) according to the manufacturer's protocol. Cells stained with annexin V-FITC and 7-AAD were analyzed by flow cytometry with a FACSCalibur (BD Bioscience, San Diego, CA, USA). Late apoptosis was evaluated by TUNEL Assay using an ApopTag fluorescein *in situ* apoptosis detection kit (Chemicon International, Inc., Temecula, CA, USA) according to the manufacturer's protocol.

Antibodies

Affinity-purified rabbit polyclonal antibody against synthetic peptides corresponding to the linker region of ZNF689 (residues 127–139) was obtained from Sigma-Aldrich (St. Louis, MO, USA). For the detection of Bcl-2 family proteins, a Pro-Apoptosis Bcl-2 Family Antibody Sampler Kit (Cell Signaling Technology, Beverly, MA, USA) and a rabbit anti-Bak antibody (Y164; Abcam, Cambridge, UK) were used. Other antibodies used were as follows: anti-FLAG (M2, Sigma) anti-β-actin (AC-15, Sigma), Anti-nucleolin (3G4B20, Millipore, Billerica, MA, USA), anti-JNK and anti-phospho-JNK (Cell Signaling Technology).

Luciferase reporter assays

Huh7 cells cultured in 12-well plates were transfected with the Bak promoter-luciferase reporter (kindly provided by Dr. Licht, Northwestern University Feinberg School of Medicine) and the internal control, pRL-CMV (Promega, Madison, WI, USA), together with or without FLAG-ZNF689-pME18S using Lipofectamine 2000 (Invitrogen). Cells were harvested at 24 h post-transfection, and

the luciferase activity was measured by a Dual-Luciferase Reporter Assay System and GLOMAX 96 microplate luminometer (Promega) according to the manufacturer's protocol.

In vivo luminescence imaging assay

HepG2 were stably labeled with green-emitting luciferases [stable luciferase green (SLG)] by a lentiviral expression system. One million SLG-expressing HepG2 cells were subcutaneously inoculated into 5-week-old female Balb/c nude mice. After 3 weeks, the tumor-bearing nude mice were treated with ZNF689 siRNA cocktail or control siRNA mixed with atelocollagen (KOKEN, Tokyo, Japan) according to the manufacturer's protocol. D-luciferin was intraperitoneally injected at the indicated day and the transplanted cells in the mice were detected by an *in vivo* bioluminescence method using AEQUORIA-2D (Hamamatsu Photonics, Hamamatsu, Japan). All mice received standard care, and our study protocol was approved by the Ethics Committee of the Graduate School of Medicine, Ehime University, Japan.

Human liver specimens

Paraffin-embedded formalin fixed human liver tissues were obtained by surgical resection of 12 cases of HCCs. Sections were 4–6 μm thick. The Ethics Committee of Ehime University approved the study protocol. Written informed consent was obtained prior to enrolment in accordance with the principles of the Declaration of Helsinki (Approval No. 0809006).

Results

Knockdown of the ZNF689 gene induced apoptosis in HCC cells in a caspase-dependent manner

To examine the role of ZNF689 in HCC cell lines, we first assessed the viability of Huh7 by the siRNA-mediated knockdown of ZNF689. Down-regulation of ZNF689 expression by siRNA was validated by quantitative-polymerase chain reaction (qPCR) and

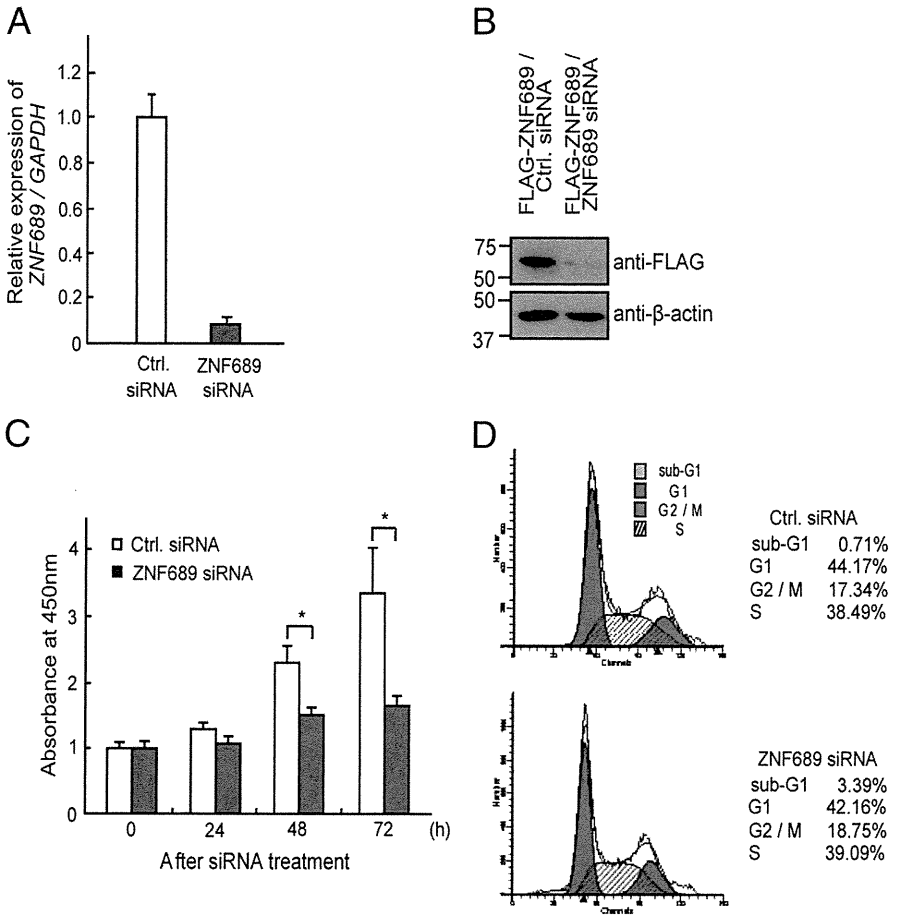

Fig. 1 – Effects of the knockdown of ZNF689 on the cell viability and cell cycle of the HCC cell line, Huh7. A. Knockdown efficiency of ZNF689 by its specific siRNA. Huh7 was transfected with either control (white bars) or ZNF689-specific (gray bars) siRNA. The expression of ZNF689 mRNA was quantified by qPCR and normalized by the expression of GAPDH as the internal control. B. Effects of siRNA against ZNF689 protein was examined by Western blot analysis. After 2 days of FLAG-ZNF689 transfection, Huh7 was further transfected with either control or ZNF689 siRNA. FLAG-ZNF689 was detected by using anti-FLAG antibody. C. Viability of control siRNA- and ZNF689 siRNA-transfected cells. Huh7 was transfected with either the control (white bars) or ZNF689-specific (gray bars) siRNA, and cell viability was measured by WST-1 assay at the indicated time points. The asterisk indicates $p < 0.05$. D. FACS analysis of Huh7 transfected with either the control (upper panel) or ZNF689 (lower panel) siRNA. The siRNA-transfected cells were stained with propidium iodide and the cell cycle was examined by FACS analysis.

Western blot analyses (Figs. 1A and B). We found that the viability of Huh7 decreased significantly 48 to 72 h after the transfection of ZNF689 siRNA (Fig. 1C). We further stained Huh7 with propidium iodide (PI) and analyzed the cell cycle stages by FACS 72 h after siRNA transfection. Although the overall cell cycle was not altered between the control and the ZNF689 siRNA-transfected cells, the proportion of the sub-G1 population was different, showing 3.39% and 0.71% in ZNF689 knockdown cells and control cells, respectively (Fig. 1D). Forty-eight hours after transfection, we observed an increased number of annexin V-positive cells in ZNF689 knocked-down cells (Fig. 2A). Furthermore, TUNEL-positive cells also increased at 72–96 h after the transfection (Figs. 2B and C). Thus, we assumed that the increase of the sub-G1 population caused by ZNF689 siRNA was due to the apoptosis of Huh7 cells.

To examine whether ZNF689 knockdown-induced cell death was caused by caspase-dependent apoptosis [11], Huh7 was transfected with siRNA and cultured in the presence of a pan-caspase inhibitor, Z-VAD-fmk. Z-VAD-fmk significantly suppressed the appearance of TUNEL-positive cells induced by ZNF689 siRNA (Figs. 3A and B). Furthermore, as judged by a tetrazolium salt (WST-1) assay in Huh7 cells, cell viability was partially, but significantly, restored by the use of Z-VAD-fmk (Fig. 3C), indicating that the caspase-dependent pathway is involved in ZNF689 knockdown-induced apoptosis.

We also confirmed the effect of ZNF689 siRNA on other HCC cell lines HepG2 and Hep3B cells. ZNF689 siRNA effectively knocked down ZNF689 mRNA in HepG2 and Hep3B cells, and increased the number of TUNEL-positive cells in both of the cells to a similar extent as that in Huh7 cells, which were significantly blocked with Z-VAD-fmk (Figs. S1A–C).

Taken together, these data suggest that the role of ZNF689 is to suppress the apoptosis of HCC cells through regulation of the caspase-dependent signaling pathway.

ZNF689 negatively regulates Bcl-2 family pro-apoptotic factors

It is known that caspase-dependent apoptosis occurs through two major pathways. One is the extrinsic pathway which involves the stimulation of members of the TNF, Fas or TRAIL receptors. The other is the intrinsic pathway in which a range of BH3-only proteins act as sentinels for cell stress [11]. The BH3-only proteins induce apoptosis by increasing mitochondrial outer membrane permeability, resulting in the release of cytochrome c [12]. In order to analyze the function of ZNF689 in these caspase-dependent pathways, we first compared gene expression profiles of apoptosis-related genes between the ZNF689 siRNA- and control siRNA-transfected Huh7 cells using real-time PCR arrays. Since ZNF689 is identified as a member of the KRAB-zinc finger family of transcriptional repressors, we especially focused on pro-apoptotic genes that were suppressed under the steady-state and up-regulated by siRNA-mediated knockdown. qPCR analysis revealed that ZNF689 siRNA up-regulated the expression of the pro-apoptotic genes Bak and Bax in comparison with the control siRNA in Huh7 (Figs. 4A and B). We also examined the effects of ZNF689 siRNA on the expression of the pro-apoptotic genes Bak and Bax in HepG2 and Hep3B cells. After the transfection of ZNF689 siRNA, Bak mRNA increased with statistical significance in both of the cells, while Bax mRNA increased with statistical significance in HepG2 (Figs. S1D and E).

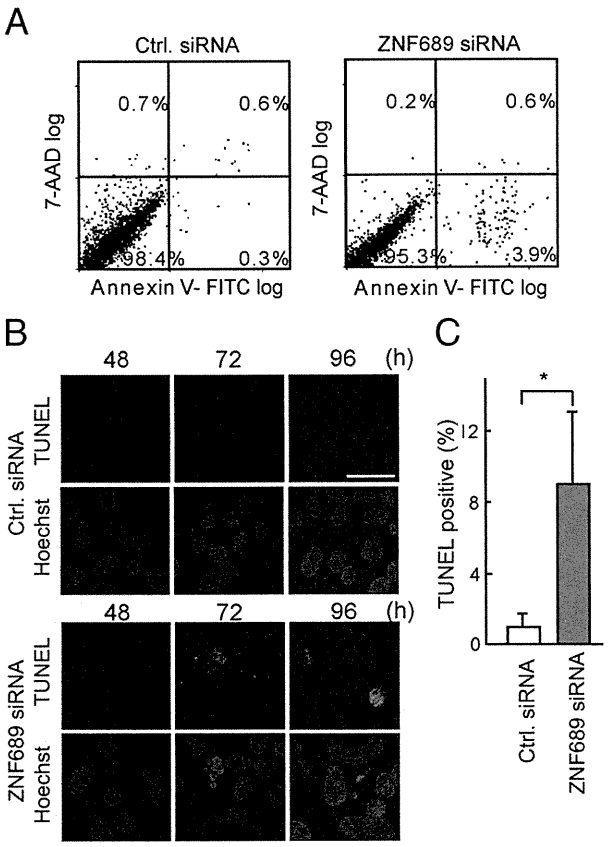

Fig. 2 – Knockdown of the ZNF689 expression induces apoptosis of Huh7. A. Early apoptosis of siRNA-treated Huh7. After the transfection of siRNA, cells were stained with Annexin V-FITC and 7-AAD, and analyzed by FACS. B. Late apoptosis of siRNA-treated Huh7. After the transfection of siRNA, TUNEL assay was performed at the indicated points. Nuclei were stained with Hoechst33342. Scale bar, 10 μm. C. The ratio of TUNEL-positive cells of control and ZNF689 siRNA-treated cells. TUNEL-positive cells shown in B were quantified. The asterisk indicates statistical significance ($p<0.05$).

Furthermore, we comprehensively examined the expression of pro-apoptotic Bcl-2 family proteins by Western blot analysis, and found the up-regulation of Bak and Bax proteins (Fig. 4C). To examine the activity of ZNF689 as a transcriptional repressor, we performed a luciferase assay using the Bak promoter [13], and found that ZNF689 significantly suppressed the promoter activity of the Bak gene (Fig. 4D). In addition, unexpectedly, jBid, one of the activated forms of Bid, was detected in ZNF689 siRNA-transfected Huh7 cells (Fig. 4C). Although the protease responsible for the processing of Bid has not been identified, it has been shown that jBid is generated by the JNK-dependent pathway [14]. We therefore assessed the activation of JNK, and found that the phosphorylated form of JNK increased in Huh7 cells transfected with ZNF689 siRNA (Fig. 4E). Furthermore, exposure of Huh7 to an apoptosis inducer, Nutlin-3, enhanced the extent of ZNF689 knockdown-mediated apoptosis, confirming that ZNF689 actually upregulates the expression of pro-apoptotic factors (Fig. 4F).

These results suggest that ZNF689 inhibits apoptosis through suppression of the expression of Bak/Bax and the appearance of

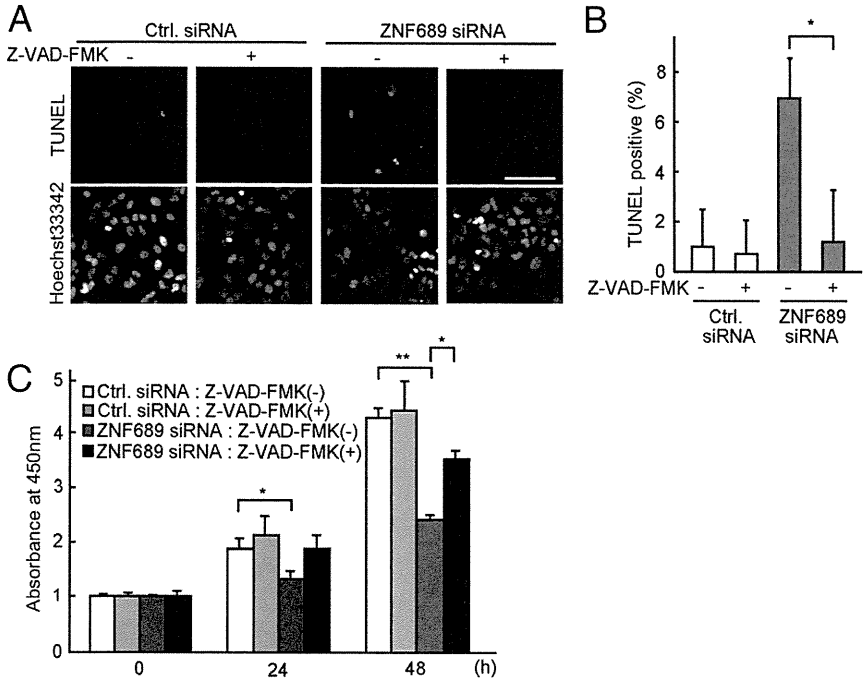

Fig. 3 – Pan-caspase inhibitor restores ZNF689-regulated cell death. A. Effects of the knockdown of ZNF689 and the Z-VAD-fmk treatment on Huh7. Control or ZNF689 siRNA-transfected Huh7 was treated with Z-VAD-FMK (20 nM). After 24 h incubation, apoptotic cells were detected by TUNEL assay. Nuclei were stained with Hoechst33342. Scale bar, 100 μm. B. The ratio of TUNEL-positive cells in A was quantified. The asterisk indicates $p < 0.05$. C. Cell viability of control or ZNF689 siRNA-transfected cells in the presence of Z-VAD-fmk. WST-1 assay was performed at the indicated time points. The asterisk indicates $p < 0.05$. Two asterisks indicate $p < 0.01$.

jBid. In the case of Bak regulation, ZNF 689 acts on the Bak promoter and represses its expression at the transcriptional level.

Correlation between the expression of ZNF689 and 5-FU resistance of HCC cells

Furthermore, we examined whether ZNF689 has a possible role in the anticancer drug resistance of HCC cells or not. We cultured Huh7 cells in the presence or absence of 5-fluorouracil (5-FU), commonly used for HCC chemotherapy. We analyzed the expression level of ZNF689 mRNA 1 week after the 5-FU addition when an arrest of cell proliferation was observed (Fig. 5A). Total RNA isolated from surviving Huh7 was examined by qPCR analysis, revealing an approximately three-fold increase of ZNF689 mRNA expression within 2 weeks of incubation (Fig. 5A). The up-regulation of ZNF689 mRNA was also observed in 5-FU-treated HepG2 and Hep3B to a different extent (Fig. S1F).

To examine the role of ZNF689 in 5-FU resistance of HCC, we knocked down the expression of ZNF689, and found that the viability of Huh7 in the presence of 5-FU decreased significantly as assessed by the WST-1 assay (Fig. 5B). The half maximal effective concentration (EC_{50}) value of 5-FU was 2.45 ± 0.42 μg/ml in control siRNA-transfected cells and 0.84 ± 0.55 μg/ml in ZNF689 siRNA-transfected cells ($p < 0.05$) (data not shown). Conversely, the EC_{50} value of 5-FU increased when ZNF689 was 5.46 ± 0.82 μg/ml in the control cells and 8.08 ± 1.30 μg/μl in ZNF689-overexpressed cells ($p < 0.05$) (data not shown).

Although the precise molecular mechanism underlying the increase of ZNF689 expression after the 5-FU treatment is unknown, we speculate that (1) 5-FU directly affects and upregulates the expression of ZNF689 gene, or (2) the 5-FU-resistant population in HCCs expresses higher amounts of ZNF689 than the 5-FU-sensitive population. These results suggested a correlation between the expression level of ZNF689 and 5-FU resistance in HCC cells, and implied that ZNF689 might have protective activity against anticancer agents.

Physiological role of ZNF689 in HCC-transplanted mice and human hepatocellular carcinoma surgical specimens

To understand the physiological role of ZNF689 *in vivo*, Huh7 and HepG2 cells stably labeled with a luciferase reporter were established and subcutaneously inoculated into nude mice. After 3 weeks, we detected tumor mass of HepG2, but not Huh7, by bioluminescence imaging. We then treated the HepG2 tumor-bearing nude mice with either ZNF689 siRNA or control siRNA (Fig. 6A). Under the experimental conditions we used, bioluminescent signals were significantly suppressed by ZNF689 siRNA compared with the control siRNA (Fig. 6B). These results suggest that ZNF689 affects the cell viability of HCC in transplanted mice as well as cultured HCC.

Finally, we raised polyclonal antibodies against a linker peptide of ZNF689 (amino acids 127–139). Although endogenous ZNF689 in Huh7 and HepG2 was undetectable by Western blot analysis using our anti-ZNF689 antibody, this antibody specifically recognized exogenously expressed ZNF689 tagged with a FLAG epitope as a single band (Fig. 6C). We immunostained FLAG-ZNF689 in Huh7 cells, and found that the FLAG-ZNF689 protein colocalized

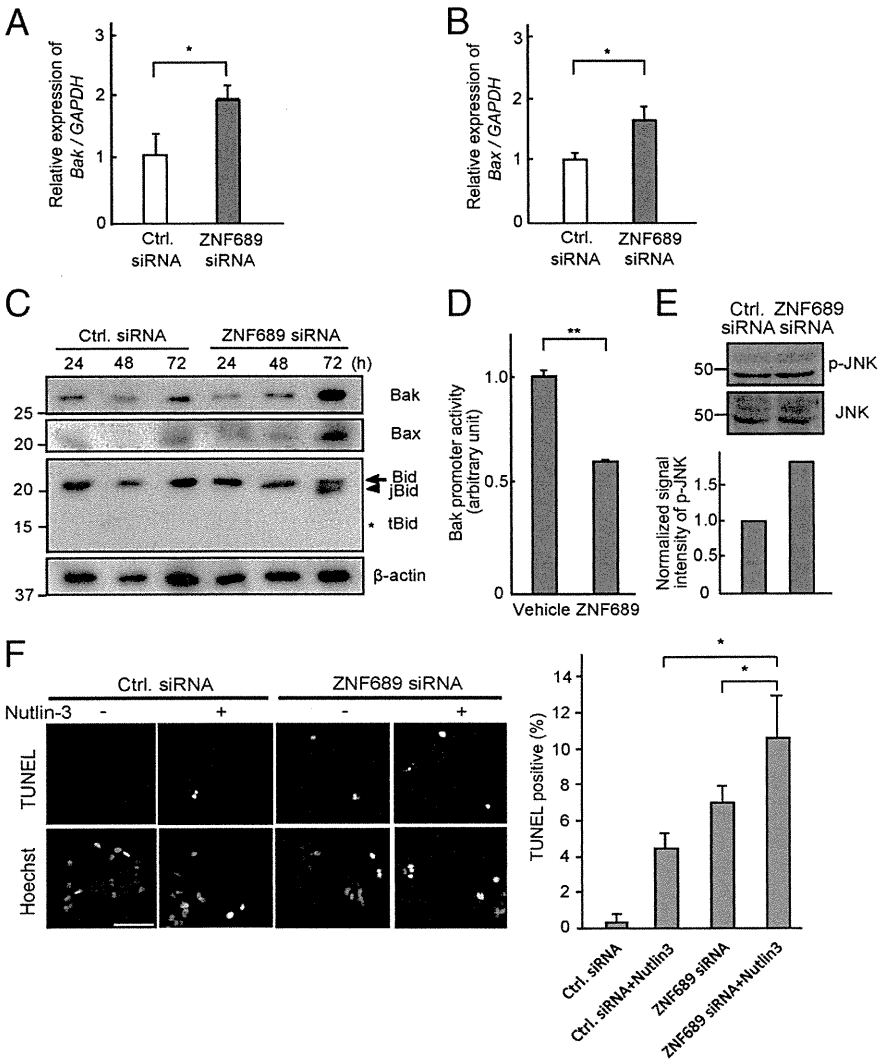

Fig. 4 – ZNF689 suppresses apoptosis through the negative regulation of apoptosis-promoting proteins. A. Upregulation of Bak mRNA expression by the knockdown of ZNF689. Total RNAs were isolated from Huh7 72 h after the transfection of either control (white bars) or ZNF689-specific (gray bars) siRNAs. The expression of Bak mRNA was quantified by qPCR and normalized by the expression of GAPDH as the internal control. B. The expression of Bax mRNA was quantified and normalized as in (A). C. Expression of Bcl-2 members of pro-apoptotic factors. Huh7 was transfected with either the control or ZNF689 siRNA, and cell lysates were prepared after the indicated time points. The expression of Bak, Bax, and Bid was examined by Western blot analysis. Full-length Bid and jBid are indicated by arrow and arrowhead, respectively. Asterisk indicates the molecular weight of tBid. β-actin was used as a loading control. D. ZNF689 suppresses the activation of Bak promoter activity. Huh7 cells were transfected with the Bak promoter-luciferase reporter plasmid and the internal control plasmid, together with or without the ZNF689-expression plasmid. After 24 h incubation, luciferase activity was measured. Two asterisks indicate $p < 0.01$. E. Phosphorylation of JNK in control or ZNF689 siRNA-treated Huh7. Band intensity of phosphorylated JNK was normalized by that of total JNK. F. Nutlin-3 enhanced ZNF689 knockdown-induced apoptosis. Control or ZNF689 siRNA-transfected Huh7 was treated with Nutlin-3 (2.5 μM). After 24 h incubation, apoptotic cells were detected by TUNEL assay. Nuclei were stained with Hoechst33342. TUNEL-positive cells in control and ZNF689 siRNA-treated cells were quantified and shown in right. Scale bar: 100 μm. The asterisk indicates statistical significance ($P < 0.05$).

with nucleolin, a nucleolus protein previously identified as a binding protein of ZNF689 (Fig. 6C). Immunohistochemical analysis using this antibody demonstrated that nuclei positive for ZNF689 were on the tumor margin or daughter nodules where cancer proliferates rapidly (Fig. 6D). In total, 25% of human HCC surgical specimens (4 of 12 cases) were positive for nuclear ZNF689.

Discussion

The development of novel HCC therapies requires understanding the molecules involved in hepatocarcinogenesis and the design of effective agents against responsible factors. The gene encoding ZNF689 was identified as up-regulated by a cDNA microarray analysis

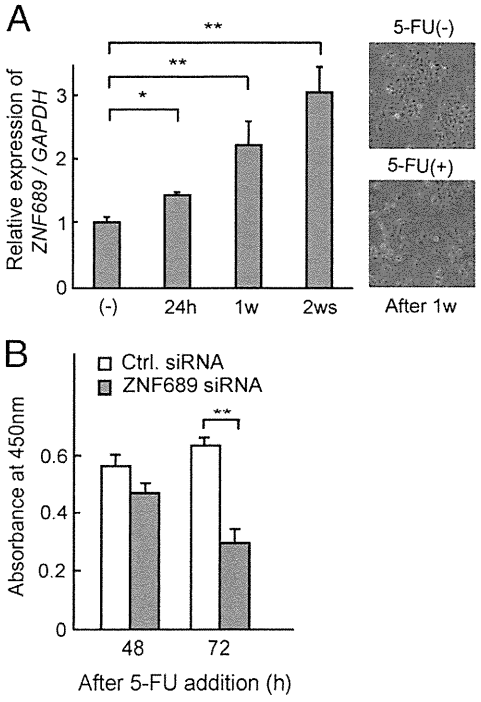

Fig. 5 – Correlation between the expression of ZNF689 and the 5-FU resistance. A. Time-course of ZNF689 mRNA levels in Huh7 following the 5-FU treatment (2 μg/ml). Total RNA of Huh7 was isolated after the 5-FU treatment at the indicated time points. The expression of ZNF689 mRNA was quantified by qPCR using GAPDH as the internal control. Right panels show bright field images of untreated and 5-FU-treated Huh7 after 1 week. B. Viability of control and ZNF689 siRNA-transfected cells in the presence of 5-FU. siRNA-transfected cells were cultured in the presence of 5-FU, and cell viability was measured by WST-1 assay. Two asterisks indicate $p < 0.01$.

of 20 human HCC tissues (termed as transcription-involved protein up-regulated in HCC: TIPUH1) [10]. Its protein, ZNF689, is a potential candidate for understanding the molecular mechanisms of hepatocarcinogenesis, as well as for diagnosis and therapy of HCC. Functional assessment of ZNF689 has primarily revealed that it has oncogenic activity in colony-formation assays in soft agar, and that it interacts with TIF1β, hnRNPU, hnRNPF, and nucleolin [10]. TIF1β is a transcriptional corepressor that recruits the histone deacetylase (HDAC) complex to DNA [15], and hnRNPU, hnRNPF, and nucleolin are all involved in mRNA or rRNA processing [16,17], suggesting that ZNF689 might regulate transcription repression and/or modification of RNA processing of genes essential for cell growth control [10]. However, none of the target genes or potential roles of ZNF689 have been elucidated to date.

In the present study, we characterized ZNF689 as an anti-apoptotic factor that modulates the apoptotic signaling cascade involving the Bcl-2 family of pro-apoptotic factors. Bak and Bax, members of the Bcl-2 family, are indispensable for apoptosis via the mitochondrial pathway, and apoptotic resistance is observed in Bak/Bax double knockout mice [18,19]. In a luciferase assay, ZNF689 suppressed the activation of the Bak promoter (Fig. 4D). Since ZNF689 has a transcriptional repression module, the KRAB domain [20], at its N-terminus, it is conceivable that ZNF689-mediated transcriptional repression is caused by its binding partner, TIF1β, and the recruitment of HDAC to the promoter region of the Bak gene. On the other hand, it is well known that another Bcl-2 member, Bid, is cleaved by caspase 8 for the generation of a 15-kDa protein, tBid [21], which drives the insertion of Bax into the membrane bilayer and oligomerization of Bax/Bak [12,22]. Treatment of Huh7 with ZNF689 siRNA generated a specific Bid antibody-reactive product migrating below the full-length Bid. Unexpectedly, it differed from tBid as judged from the molecular weight, and instead corresponded to a previously reported form of Bid, jBid. To date, only a single report is available for jBid, underscoring the lack of information on how jBid is processed from Bid [14]. Since we observed an increase of phosphorylated JNK in ZNF689 knockdown cells, ZNF689 might act on regulatory factor(s) upstream of JNK through transcriptional regulation. Further analysis of ZNF689 is necessary to elucidate the protease(s) activated by phosphorylated JNK, and the details of the unidentified component of the Bid-mediated pro-apoptotic pathway.

Accumulated evidence suggests an association between quantitative and qualitative defects in ribosome biogenesis and neoplastic transformation [23]. Up-regulation of hepatocyte ribosome biogenesis is consistently associated with later onset of HCC [24,25]. There is now evidence that proto-oncogene c-Myc binds to human ribosomal DNA and enhances RNA polymerase I transcriptional activity [26,27]. Since immunocytochemistry revealed that ZNF689 is localized in the nucleolus, and co-localizes with nucleolin, a ubiquitous eukaryotic protein essential for pre-ribosome assembly (Fig. 6C), up-regulated expression of ZNF689 may contribute to ribosome biogenesis of HCC through a physical interaction with nucleolin.

Silva et al. also showed that ZNF689 is highly expressed in HCC, but not in corresponding non-cancerous tissues [10]. They also remarked that targeting ZNF689 with anti-HCC drugs may be relatively safe because its expression is weak or absent in normal adult human tissues, except for the testis and placenta. Our preliminary study indicates that the expression of ZNF689 is not limited to HCC, but is also detected in a broad range of established cancer cell lines, such as human fibrosarcoma HT1080, cervical carcinoma cell line HeLa, and breast cancer cell line MCF7. In contrast, and consistent with previous observations, qPCR analysis showed that the expression of ZNF689 is extremely low in untransformed cells such as primary human hepatocytes, keratinocytes, and human umbilical vein endothelial cells (HUVEC) (data not shown). Therefore, ZNF689-mediated anti-apoptotic effects may have a more general role in the development of a wide variety of cancers.

In conclusion, we unveiled the anti-apoptotic mechanism of ZNF689 and propose that HCC cells that express ZNF689 at a high level can avoid cell death from chemotherapeutic drugs and proliferate. Our results suggest that siRNA against ZNF689 could be a crucial treatment for HCC, especially in the context of 5-FU-based combination chemotherapy. Further characterization of ZNF689 focusing on the apoptotic signaling pathway in HCC would improve understanding of proliferation and resistance to anticancer agents acquired by normal hepatocytes.

Supplementary materials related to this article can be found online at doi:10.1016/j.yexcr.2011.05.012.

Conflict of interest

The authors declare no conflict of interest.

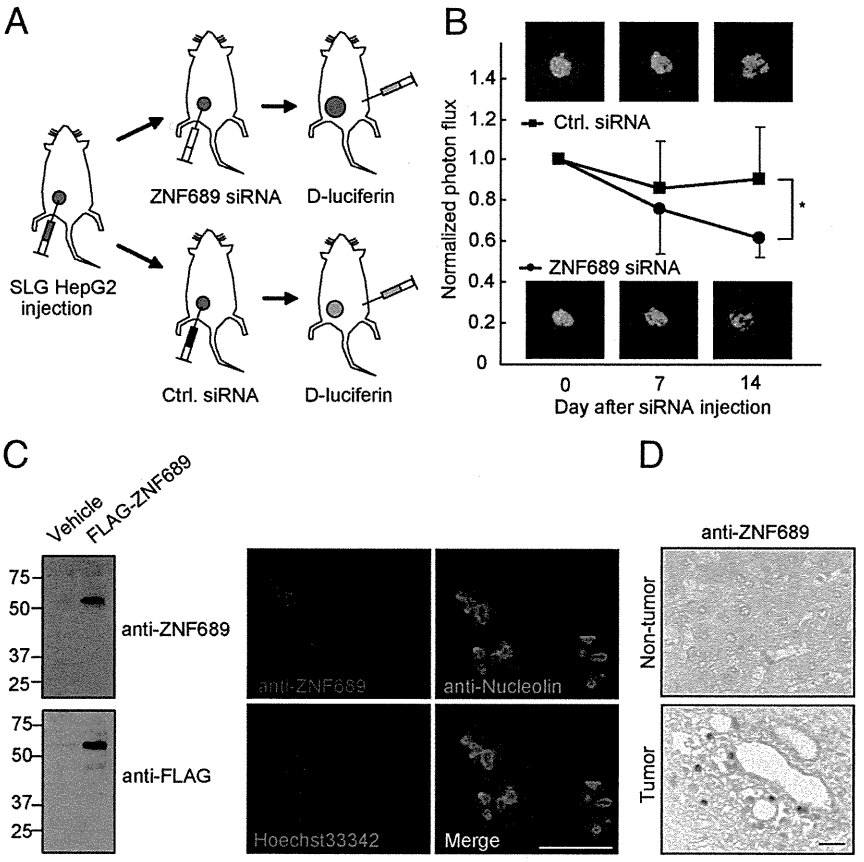

Fig. 6 – Physiological role of ZNF689 in HCC-transplanted mice and human hepatocellular carcinoma surgical specimens. A. Diagram of the seeding experiment. Luciferase-expressing liver cancer cells (SLG-HepG2) were subcutaneously injected into nude mice. When tumors were observed by bioluminescence imaging, siRNA was injected into the tumor at a final concentration of 10 nM. B. Luminescent signals of seeded tumors at the indicated time points. Color-range indicates photon flux. n = 4–5. The asterisk indicates $p < 0.05$. C. ZNF689 localized in the nucleolus. Antibody against the linker region of ZNF689 was used for Western blot analysis and immunocytochemistry. The antibody detected exogenous FLAG-tagged ZNF689 as a single band in Huh7 cells (left panels). Nucleoli and nuclei were detected by anti-Nucleolin antibody and Hoechst33342, respectively. Scale bar, 10 μm. D. Detection of the ZNF689 protein in the nucleus of hepatocellular surgical specimens. Scale bar, 10 μm.

Acknowledgments

We thank Dr. Licht (Northwestern University Feinberg School of Medicine) for kindly providing the Bak promoter-luciferase reporter plasmid and Dr. Tanimoto (Ehime University Graduate School of Medicine) for the staining of human liver specimen. We also thank members of Higashiyama and Onji laboratories for technical assistance, helpful comments, and discussion. This work was supported by Grant-in-Aid for Scientific Research (no. 17014068 and no. 20390082) to S. Higashiyama, and also supported in part by Program for Enhancing Systematic Education in Graduate School, from the Ministry of Education, Culture, Sports, Science, and Technology, Japan.

REFERENCES

[1] A.S. Befeler, A.M. Di Bisceglie, Hepatocellular carcinoma: diagnosis and treatment, Gastroenterology 122 (2002) 1609–1619.

[2] J. Bruix, M. Sherman, Management of hepatocellular carcinoma, Hepatology 42 (2005) 1208–1236.

[3] M.A. Avila, C. Berasain, B. Sangro, J. Prieto, New therapies for hepatocellular carcinoma, Oncogene 25 (2006) 3866–3884.

[4] C. Berasain, J. Castillo, M.J. Perugorria, M.U. Latasa, J. Prieto, M.A. Avila, Inflammation and liver cancer: new molecular links, Ann. N. Y. Acad. Sci. 1155 (2009) 206–221.

[5] Y. Inui, S. Higashiyama, S. Kawata, S. Tamura, J. Miyagawa, N. Taniguchi, Y. Matsuzawa, Expression of heparin-binding epidermal growth factor in human hepatocellular carcinoma, Gastroenterology 107 (1994) 1799–1804.

[6] D. Nanba, A. Mammoto, K. Hashimoto, S. Higashiyama, Proteolytic release of the carboxy-terminal fragment of proHB-EGF causes nuclear export of PLZF, J. Cell Biol. 163 (2003) 489–502.

[7] M. Hieda, M. Isokane, M. Koizumi, C. Higashi, T. Tachibana, M. Shudou, T. Taguchi, Y. Hieda, S. Higashiyama, Membrane-anchored growth factor, HB-EGF, on the cell surface targeted to the inner nuclear membrane, J. Cell Biol. 180 (2008) 763–769.

[8] Y. Kinugasa, M. Hieda, M. Hori, S. Higashiyama, The carboxyl-terminal fragment of pro-HB-EGF reverses Bcl6-mediated gene repression, J. Biol. Chem. 282 (2007) 14797–14806.

[9] W.H. Su, C.C. Chao, S.H. Yeh, D.S. Chen, P.J. Chen, Y.S. Jou, D.B. Onco, HCC: an integrated oncogenomic database of hepatocellular carcinoma revealed aberrant cancer target genes and loci, Nucleic Acids Res. 35 (2007) D727–D731.
[10] F.P. Silva, R. Hamamoto, Y. Furukawa, Y. Nakamura, TIPUH1 encodes a novel KRAB zinc-finger protein highly expressed in human hepatocellular carcinomas, Oncogene 25 (2006) 5063–5070.
[11] G. Kroemer, S.J. Martin, Caspase-independent cell death, Nat. Med. 11 (2005) 725–730.
[12] H. Puthalakath, A. Strasser, Keeping killers on a tight leash: transcriptional and post-translational control of the pro-apoptotic activity of BH3-only proteins, Cell Death Differ. 9 (2002) 505–512.
[13] D.J. Morrison, M.A. English, J.D. Licht, WT1 induces apoptosis through transcriptional regulation of the proapoptotic Bcl-2 family member Bak, Cancer Res. 65 (2005) 8174–8182.
[14] Y. Deng, X. Ren, L. Yang, Y. Lin, X. Wu, A JNK-dependent pathway is required for TNFalpha-induced apoptosis, Cell 115 (2003) 61–70.
[15] D.C. Schultz, J.R. Friedman, F.J. Rauscher III, Targeting histone deacetylase complexes via KRAB-zinc finger proteins: the PHD and bromodomains of KAP-1 form a cooperative unit that recruits a novel isoform of the Mi-2alpha subunit of NuRD, Genes Dev. 15 (2001) 428–443.
[16] R. Reed, K. Magni, A new view of mRNA export: separating the wheat from the chaff, Nat. Cell Biol. 3 (2001) E201–E204.
[17] M. Srivastava, H.B. Pollard, Molecular dissection of nucleolin's role in growth and cell proliferation: new insights, FASEB J. 13 (1999) 1911–1922.
[18] T. Lindsten, A.J. Ross, A. King, W.X. Zong, J.C. Rathmell, H.A. Shiels, E. Ulrich, K.G. Waymire, P. Mahar, K. Frauwirth, Y. Chen, M. Wei, V.M. Eng, D.M. Adelman, M.C. Simon, A. Ma, J.A. Golden, G. Evan, S.J. Korsmeyer, G.R. MacGregor, C.B. Thompson, The combined functions of proapoptotic Bcl-2 family members bak and bax are essential for normal development of multiple tissues, Mol. Cell 6 (2000) 1389–1399.
[19] M.C. Wei, W.X. Zong, E.H. Cheng, T. Lindsten, V. Panoutsakopoulou, A.J. Ross, K.A. Roth, G.R. MacGregor, C.B. Thompson, S.J. Korsmeyer, Proapoptotic BAX and BAK: a requisite gateway to mitochondrial dysfunction and death, Science 292 (2001) 727–730.
[20] R. Urrutia, KRAB-containing zinc-finger repressor proteins, Genome Biol. 4 (2003) 231.
[21] M.D. Esposti, The roles of Bid, Apoptosis 7 (2002) 433–440.
[22] L.P. Billen, A. Shamas-Din, D.W. Andrews, Bid: a Bax-like BH3 protein, Oncogene 27 (Suppl. 1) (2008) S93–S104.
[23] L. Montanaro, D. Trere, M. Derenzini, Nucleolus, ribosomes, and cancer, Am. J. Pathol. 173 (2008) 301–310.
[24] M. Derenzini, D. Trere, F. Oliveri, E. David, P. Colombatto, F. Bonino, M.R. Brunetto, Is high AgNOR quantity in hepatocytes associated with increased risk of hepatocellular carcinoma in chronic liver disease? J. Clin. Pathol. 46 (1993) 727–729.
[25] D. Trere, M. Borzio, A. Morabito, F. Borzio, M. Roncalli, M. Derenzini, Nucleolar hypertrophy correlates with hepatocellular carcinoma development in cirrhosis due to HBV infection, Hepatology 37 (2003) 72–78.
[26] A. Arabi, S. Wu, K. Ridderstrale, H. Bierhoff, C. Shiue, K. Fatyol, S. Fahlen, P. Hydbring, O. Soderberg, I. Grummt, L.G. Larsson, A.P. Wright, c-Myc associates with ribosomal DNA and activates RNA polymerase I transcription, Nat. Cell Biol. 7 (2005) 303–310.
[27] C. Grandori, N. Gomez-Roman, Z.A. Felton-Edkins, C. Ngouenet, D.A. Galloway, R.N. Eisenman, R.J. White, c-Myc binds to human ribosomal DNA and stimulates transcription of rRNA genes by RNA polymerase I, Nat. Cell Biol. 7 (2005) 311–318.

Hepatic Elasticity in Patients With Ascites: Evaluation With Real-Time Tissue Elastography

Masashi Hirooka[1]
Yohei Koizumi
Yoichi Hiasa
Masanori Abe
Yoshio Ikeda
Bunzo Matsuura
Morikazu Onji

OBJECTIVE. Transient elastography is a rapid, noninvasive, and reproducible approach to assessment of liver fibrosis by measurement of liver elasticity. However, transient elastographic measurements are of limited utility in patients with ascites or severe obesity. The aim of this study was to determine whether measurements of liver stiffness with real-time tissue elastography can be altered for patients with ascites.

SUBJECTS AND METHODS. The subjects were 54 patients being treated at a university hospital between January and December 2009. In 42 patients, real-time tissue elastography to evaluate liver stiffness was performed before and after injection to produce artificial ascites for radiofrequency ablation. The other 12 patients had ascites due to cirrhosis, and liver stiffness was measured with real-time tissue elastography before and after control of ascites.

RESULTS. Elastic ratios evaluated with real-time tissue elastography did not differ significantly before and after injection for artificial ascites or before and after control of ascites. This ratio was the same for patients with and those without cirrhosis and was unaffected by distance between the body surface and the targeted liver area. Stable values thus were measured with real-time tissue elastography.

CONCLUSION. Liver stiffness can be measured reproducibly with real-time tissue elastography even in patients with ascites. This method has the potential of being superior to transient elastography for assessment of liver stiffness, particularly in patients with decompensated cirrhosis.

Keywords: ascites, elastic ratio, liver stiffness, real-time tissue elastography, reproducibility

DOI:10.2214/AJR.10.4867

Received April 21, 2010; accepted after revision October 11, 2010.

Supported in part by a grant-in-aid for scientific research (JSPS KAKENHI 21590848) to Y. Hiasa from the Japanese Ministry of Education, Culture, Sports, Science and Technology.

[1]All authors: Department of Gastroenterology and Metabology, Ehime University Graduate School of Medicine, Shitsukawa, Toon, Ehime 791-0295, Japan. Address correspondence to Y. Hiasa (hiasa@m.ehime-u.ac.jp).

WEB
This is a Web exclusive article.

AJR 2011; 196:W766–W771

0361–803X/11/1966–W766

Liver biopsy is considered the reference standard for evaluation of hepatic fibrosis. However, this procedure is invasive and carries risk of life-threatening complications [1]. In addition, the reproducibility of liver biopsy in the assessment of fibrosis is limited because of sampling error and interobserver variability [2–6]. Transient elastography is a rapid, noninvasive, and reproducible approach to the assessment of liver fibrosis through the measurement of liver elasticity [7, 8]. Liver stiffness measured with transient elastography is associated strongly with the degree of liver fibrosis in patients with chronic hepatitis [9–12]. Although the accumulation of fibrillar extracellular matrix is certainly a major determinant of liver tissue stiffness during transient elastography, other factors associated with chronic liver disease, such as inflammatory infiltration, tissue necrosis, and edema, may affect the evaluation [13, 14]. Moreover, transient elastographic measurement is known to be limited in patients with severe obesity or ascites [15], and previous studies of transient elastography have excluded patients with ascites [3–6]. Ascites is a physical limitation to push-pulse technique because elastic waves do not propagate through liquids.

Investigations of transient elastography and real-time tissue elastography have proved the utility of noninvasive assessment of liver tissue stiffness in patients with chronic liver disease, such as viral hepatitis and cirrhosis [16]. Real-time tissue elastography is performed with B-mode sonography, and the method by which elasticity is measured with real-time tissue elastography differs from the method of transient elastography. Real-time tissue elastography has more potential for precise evaluation of liver stiffness than does transient elastography because, first, numerous pulses are transmitted and mean values of the frames are used and, second, elasticity can be measured with slight compression or

TABLE 1: Clinical Characteristics

Characteristic	Total (n = 54)	Artificial Ascites Group (n = 42)	Ascites Group (n = 12)
Male to female ratio	41/13	33/9	8/4
Age (y)	66.3 ± 8.0	66.0 ± 8.7	67.3 ± 4.8
Serologic findings			
Hepatic B surface antigen positive	10	7	3
Hepatitis C virus antibody positive	32	27	5
Negative both for HBs-antigen and hepatitis C virus antibody	12	8	4
Pathologic finding			
Hepatocellular carcinoma	49	37	12
Metastatic liver tumor	5	5	0
Child-Pugh class			
A	40	40	0
B	2	2	0
C	12	0	12
Metavir score[a]			
F0		5	
F1		0	
F2		3	
F3		5	
F4		29	

Note—Except for age, values are number of patients.
[a]The ascites group did not undergo biopsy.

relaxation of the body and echo signals are captured in real time. Furthermore, real-time tissue elastography can display tissue elasticity images and conventional B-mode images simultaneously. With this simultaneous display, anatomic correlations between elasticity images and B-mode images can be more readily understood than in transient elastography. The aim of the current study was to determine whether real-time tissue elastography is sufficiently precise for evaluation of liver stiffness in patients with ascites.

Subjects and Methods

Patients

The ethics committee of our institution approved all study protocols. Written informed consent to participate in the study was obtained before enrollment, in accordance with the principles of the Declaration of Helsinki. The subjects were 54 patients (41 men, 13 women; mean age, 66.3 ± 8.0 years; range, 47–81 years) treated at our institution between January and December 2009. The clinical backgrounds of the subjects are shown in Table 1. The study protocol is shown in Figure 1. Of the 54 patients, 42 patients had no ascites originally and were undergoing radiofrequency ablation of hepatocellular carcinoma and artificial ascites was being introduced in the procedure, as reported previously [16, 17]. Liver biopsy and real-time tissue elastography were performed before the artificial ascites injection. Real-time tissue elastography was repeated after induction of artificial ascites, and radiofrequency ablation was performed to manage the hepatocellular carcinoma nodule. Measurement of liver stiffness with real-time tissue elastography also was undertaken for the 12 patients who had ascites due to cirrhosis. All 12 patients had chronic liver disease diagnosed according to standard criteria with laboratory tests, sonography, CT, and endoscopy. Three patients had positive results for hepatitis B surface antigen; five had positive results for hepatitis C virus; and four had a history of alcohol abuse. Control of ascites was achieved in all 12 patients by sodium restriction and standard management of cirrhosis (diuretics with or without administration of IV albumin). Sonography was performed to confirm a decrease in ascites after these treatments. After ascites was controlled, real-time tissue elastography was repeated.

Exclusion criteria for enrollment in this study were body mass index of 25 or greater, platelet count less than 30,000/μL, use of hepatotoxic drugs in the 6 months before enrollment, vascular diseases of the liver, biliary tract disorders, cardiac failure, and pregnancy. All patients underwent laboratory tests at enrollment, including serum bilirubin, albumin, ammonia, aspartate aminotransferase, alanine aminotransferase, alkaline phosphatase, γ-glutamyl transpeptidase, platelet count, and creatinine and glucose concentrations.

Measurement of Hepatic Elasticity With Real-Time Tissue Elastography

Hepatic elasticity was measured with a real-time tissue elastographic system (EUB-7500, Hitachi Medical Systems) [18]. A linear probe (central frequency, 5.5 MHz; EUP-L52, Hitachi Medical Systems) was used. During real-time tissue elastography, B mode was used first for visualization of the liver and then elastographic mode was instituted. During elastography, areas of normal liver parenchyma appear green, and areas of increased liver stiffness appear blue (Fig. 2). Small intrahepatic vessels appear red. To reduce variation between individuals, we proposed use of the red signal as an internal control for evaluating stiffness of the liver parenchyma. We therefore first evaluated variability in the red signal in portal vessels and hepatic veins and then defined the red signal of hepatic veins as an internal control because these vessels had less variation than portal vessels.

Regions of interest were placed on small intrahepatic veins and the hepatic parenchyma at the same time, and each signal was evaluated. From those data, we calculated the ratio of the value of small

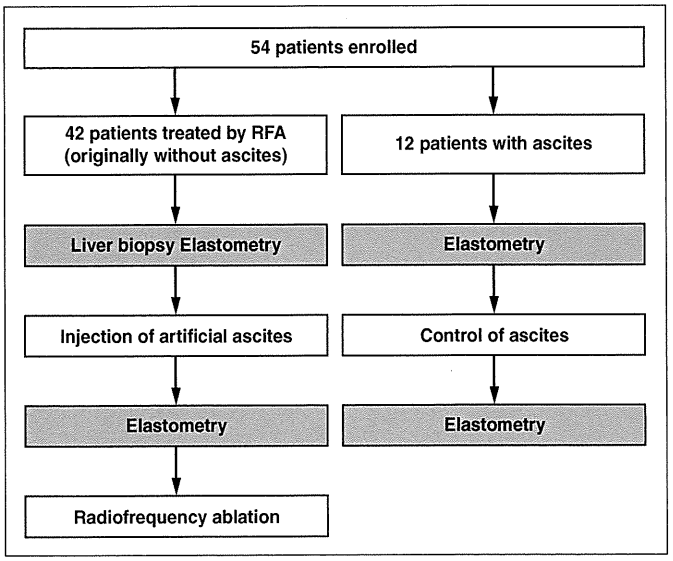

Fig. 1—Chart shows flow of participants through trial. For 42 of 54 patients, liver stiffness was measured before and after injection for artificial ascites for radiofrequency ablation (RFA). For 12 patients, who already had ascites at enrollment, real-time tissue elastography for evaluation of liver stiffness was performed before and after control of ascites.

intrahepatic veins to the value of hepatic parenchyma as the elastic ratio, a higher elastic ratio indicating greater hepatic elasticity. The region of interest placed in the liver parenchyma measured 2 × 1 cm. At the time of measurement, we placed a probe in the intercostal space. Bare minimum pressure was placed on the probe to ensure measurement universality. Because each heartbeat distorts the liver, the pressure on the liver needed for evaluation of liver stiffness with real-time tissue elastography was automatically produced by the heart. Observations were made by freehand technique, the probe being kept in position by application of slight manual pressure.

Liver Histologic Assessment

Ultrasound-guided percutaneous liver biopsy (suction technique with a needle 1.6 mm in diameter and 150 mm long) was performed before injection for artificial ascites. We excluded liver specimens shorter than 12 mm. Liver biopsy samples were fixed in formalin and embedded in paraffin. Sections 4 μm thick were stained with H and E and silver impregnation. Liver biopsy samples that contained fewer than five portal tracks (except for cirrhosis) were excluded from histologic analysis. Fibrosis was staged by two pathologists blinded to patient characteristics. The lesions were scored with the 4-point Metavir system (F0, no fibrosis; F1, portal fibrosis without septa; F2, portal fibrosis and few septa; F3, numerous septa without cirrhosis; F4, cirrhosis) [19]. Hepatitis activity was graded A0, none; A1, mild; A2, moderate; and A3, severe [20].

Injection of Ascites

All patients received premedication with an intramuscular injection of 25 mg of hydroxyzine and 15 mg of pentazocine while conscious. During each procedure, oxygen saturation and other vital signs were assessed regularly. A 14-gauge needle (Daimon Needle, Silux) with a metallic flat-cut trocar and a diamond-cut inner stylet was used for artificial ascites infusion under real-time sonographic guidance. The needle was inserted along the edge of the liver to avoid injury to the liver and adjacent organs. When the needle reached the abdominal cavity, the inner stylet was removed and 5% glucose solution was infused rapidly [16, 17]. After the area of ascites was discerned with B-mode ultrasound, liver stiffness was measured with real-time tissue elastography (Fig. 2).

Statistical Analysis

Quantitative variables are reported as mean ± SD. Differences of all variables in Tables 2 and 3 (i.e., distances from body surface to liver surface and elastic ratios) between the two groups (Fig. 3) were evaluated with the paired Student *t* test after confirmation of a normal distribution. The diagnostic performance of liver stiffness evaluation and fibrosis area was determined in terms of sensitivity, specificity, positive predictive value, negative predictive value, diagnostic reproducibility, and area under the receiver operating characteristic curve. Statistical analyses were performed with JMP software (version 8, SAS Institute Japan).

Results

The characteristics of the 42 patients (33 men, nine women; mean age, 66.0 ± 8.7 years) who underwent artificial ascites injection are shown in Table 1. The stage of liver fibrosis was F0 in five patients, F2 in three patients, F3 in five patients, and F4 in 29 patients. Forty patients had Child-Pugh class A disease, and two patients with cirrhosis had Child-Pugh class B disease. Seven patients had positive results for hepatitis B surface antigen and 27 for hepatitis C virus, and eight patients had negative results for both hepatitis B surface antigen and hepatitis C virus. Hepatocellular carcinoma nodules were identified in 37 patients, and the other five patients had metastatic liver tumors. Two nodules were located in segment IV, 23 in segment VI, two in segment VII, and 15 in segment VIII. The total volume of injected artificial ascites fluid was 1097.1 ± 199.2 mL (range, 780–1500 mL). The mean distance between the body surface and the surface of the liver was 22.5 ± 3.3 mm (range, 16.5–31.1 mm).

Among the patients who underwent artificial ascites injection, the mean elastic ratio was 3.78 ± 0.87 before injection and 3.75 ± 0.76 after injection ($p = 0.973$), not a significant

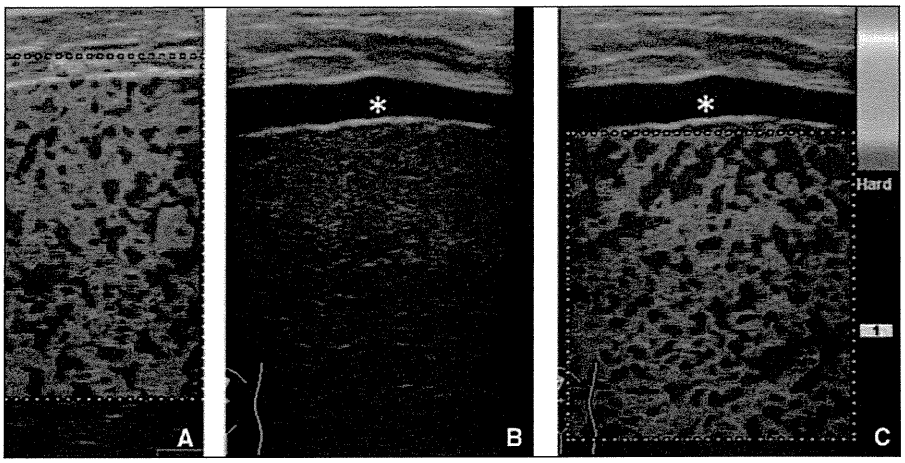

Fig. 2—54-year-old man undergoing radiofrequency ablation of hepatocellular carcinoma.
A, Tissue elastographic image before injection for artificial ascites shows elastic ratio of 2.79.
B, B-mode ultrasound image shows layer of artificial ascites (*asterisk*).
C, Tissue elastographic image shows elastic ratio of 2.80 in presence of ascites (*asterisk*).

TABLE 2: Liver Stiffness Before and After Artificial Ascites Injection

Characteristic	*n*	Before	After	Paired Difference	*p*
Distance (mm)[a]		10.51 ± 1.48	22.61 ± 3.35	12.100	< 0.0001
Elastic ratio	42	3.78 ± 0.87	3.75 ± 0.76	−0.0293	0.973
Cirrhosis[b]	29	4.22 ± 0.40	4.26 ± 0.39	−0.0355	0.980
No cirrhosis[c]	13	2.69 ± 0.62	2.70 ± 0.66	−0.0154	0.680
Elastic ratios substratified by volume of artificial ascites (mL)					
< 1000	28	3.92 ± 0.73	3.95 ± 0.75	−0.0332	0.957
≥ 1000	14	3.39 ± 0.99	3.42 ± 1.03	−0.0214	0.790

[a]Between body surface and surface of liver.
[b]Metavir F4.
[c]Metavir scores other than 4.

TABLE 3: Liver Stiffness Before and After Control of Ascites

Parameter	Before	After	Paired Difference	*p*
Distance (mm)[a]	28.48 ± 2.82	18.13 ± 2.52	18.133	< 0.0001
Elastic ratio	5.46 ± 0.52	5.51 ± 0.45	0.0533	0.766

[a]From body surface to surface of liver.

change (Fig. 3A). Moreover, the amount of ascites and the distance between the abdominal skin and the liver surface had no influence on elastic ratio (Table 2). Areas under the receiver operating characteristic curves of elastic ratios for predicting F0, greater than F2, and F4 were 1.00 ($p < 0.0001$), 0.95 ($p < 0.0001$), and 0.92 ($p < 0.0001$).

All 12 patients (eight men, four women; mean age, 67.3 ± 4.8 years) who already had ascites due to cirrhosis (Table 1) had Child-Pugh class C disease. The mean distance between the body surface and the surface of the liver was 28.4 ± 2.8 mm (range, 21.9–32.0 mm) before ascites control and was significantly lower after control. The elastic ratio was measured in all 12 patients (Table 3) and was not significantly changed after control of ascites (Table 3 and Fig. 3B). The mean interval between elastographic measurements before and after ascites control was 20.3 ± 5.8 days.

Discussion

This study confirmed that liver stiffness can be evaluated in a stable manner with real-time tissue elastography and B-mode sonography even in patients with ascites. The reference standard for assessing liver fibrosis is liver biopsy, but that technique is invasive, and many patients subsequently report pain [21]. The procedure also carries a risk of severe complications, at a rate of 3.1 cases per 1000 patients [22]. Sampling error also can complicate evaluation of liver stiffness because the biopsy specimen represents 1/50,000 of the total liver [1]. Moreover, interobserver and intraobserver discrepancies of 10–20% in assessing hepatic fibrosis have been reported [6, 23, 24], potentially contributing to the misdiagnosis of cirrhosis.

In contrast to liver biopsy, transient elastography with ultrasound is painless and carries little risk of complications. Liver stiffness is measured in a cylindric volume approximately 1 cm in diameter by 2 cm long, representing a volume 100 times larger than a biopsy specimen. Transient elastography also is more representative of the entire hepatic parenchyma [21] and is well accepted. Transient elastography does, however, have limitations in the measurement of liver stiffness. Elastometry by transient elastography cannot be used in patients with ascites, even if clinically undetected. Ascites poses a physical impediment to push-pulse technique because elastic waves do not propagate through liquids. Accurate elastic measurements thus cannot be obtained by transient elastography in patients with advanced cirrhosis because most patients with cirrhosis have ascites. In contrast, elastometry with real-time tissue elastography can be performed on patients with ascites, for the following reasons.

First, real-time tissue elastography is a combined autocorrelation method that entails color Doppler imaging [25], whereas transient elastography entails the Doppler method. In the Doppler method, which has only two signals, many pulses are transmitted, and the mean values of the frames are used. In real-

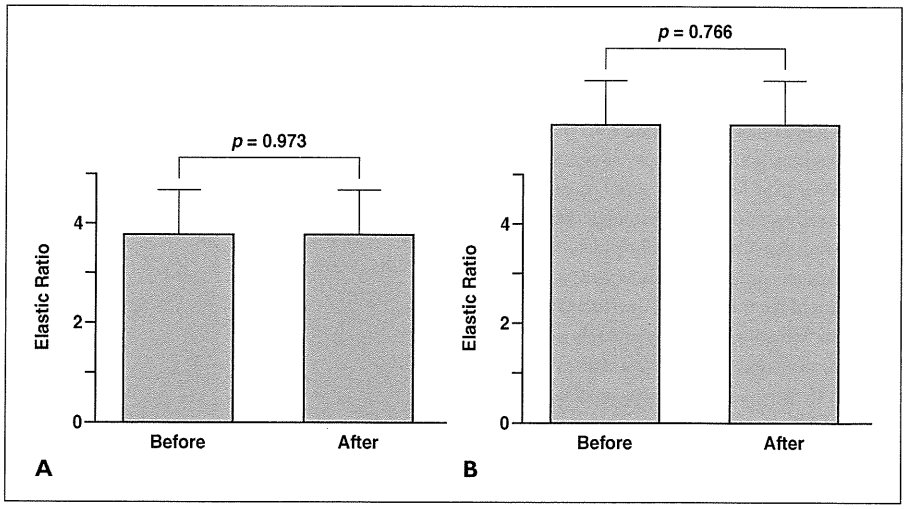

Fig. 3—Elastic ratios. No significant differences were found between real-time tissue elastographic measurements with and without ascites; *p* is based on paired Student *t* test of paired differences of ratios.
A, Graph shows results before and after artificial ascites injection.
B, Graph shows results before and after successful control of ascites.